



## Nucleation and Growth of Calcium Carbonate with Controllable Polymorphs on Solid Templates

TIAN-HUA CHEN<sup>1,2</sup>, ZHI-WU HAN<sup>1,\*</sup> and FEI LU<sup>3</sup>

<sup>1</sup>Key Laboratory for Bionic Engineering, Ministry of Education, Jilin University, Changchun 130022, P.R. China

<sup>2</sup>School of Mechanical Engineering, Changchun University, Changchun 130022, P.R. China

<sup>3</sup>Jilin Institute of Chemical Technology, Jilin City 132022, P.R. China

\*Corresponding author: Fax: +86 431 85095760- 8408; Tel: +86 431 85095760-8405; E-mail: zwhan@jlu.edu.cn

(Received: 9 July 2011;

Accepted: 9 March 2012)

AJC-11166

Controlling crystal polymorphs and crystal size is a highly important issue in many biomedical applications. In this study, Au and Si substrates were used as solid templates to control the growth of calcium carbonate ( $\text{CaCO}_3$ ) crystals. The obtained  $\text{CaCO}_3$  composite was characterized by X-ray powder diffraction, scanning electron microscopy and Fourier transform infrared spectroscopy. Results show that the solid materials can serve as templates for growing different  $\text{CaCO}_3$  crystal polymorphs. Vaterite and calcite polymorphs co-form on the template because of the presence of silanol (OH) groups in the Si substrate. Aragonite polymorphs form on the Au substrate. The possible mechanism of interaction between the template and  $\text{CaCO}_3$  growth is discussed. Results suggest that template properties are important factors in controlling crystal polymorphs.

**Key Words:** Calcium compounds, Substrates growth from solutions, Crystal morphology.

### INTRODUCTION

Polymorphism pertains to the phenomenon of molecular packing in different modes, forming two or more crystal structures<sup>1</sup>. The development of high quality crystal products necessitates comprehensive understanding and control of polymorphism because different solid forms may exhibit different physical properties such as solubility, crystal shape, dissolution rate, bioavailability and pharmacological effect<sup>2,3</sup>. For polymorphism, studying the crystallization of calcium carbonate is an interesting research direction. Calcium carbonate exhibits a variety of polymorphic modifications; three anhydrous polymorphic forms of calcite, aragonite and vaterite are generally found in nature<sup>4,5</sup>. Among these anhydrous crystalline phases, calcite is the most thermodynamically stable, whereas vaterite is the most unstable<sup>6</sup>. Furthermore, the synthesis of  $\text{CaCO}_3$  crystals has drawn considerable interest because of its potential biomedical applications, including drug delivery<sup>6</sup> and gene therapy for cancer<sup>7</sup>.

The template method<sup>8,9</sup> is a simple means of controlling the shape of  $\text{CaCO}_3$  crystals. Specifically, the geometry and dimensions of the template are critical in determining  $\text{CaCO}_3$  polymorphism because crystal growth is influenced by spatial confinement, as well as by the chemical moiety of the template. The growth of  $\text{CaCO}_3$  crystals on a range of organic molecules and templates has been extensively studied and experimented on. The Langmuir monolayer<sup>10</sup>, self-assembled monolayers<sup>11,12</sup>

and polymers<sup>13,14</sup> have all been used as substrates for  $\text{CaCO}_3$  crystal growth. Although a well-structured solid template is used for  $\text{CaCO}_3$  mineralization, in which polymorphism can be controlled, this template is usually decorated with biomolecules containing chemical functional groups<sup>15</sup>. The template can also be decorated by providing patches on it<sup>16</sup>. In the present study, untreated Au and Si substrates are selected as templates. The experimental results confirm that  $\text{CaCO}_3$  crystals with different polymorphs are successfully obtained on the substrates even though they crystallize under the same experimental conditions.

### EXPERIMENTAL

The Au(110) template was prepared by conventional repeated sputter/annealing cycles<sup>17</sup>. During sputtering, the Au crystal was bombarded for 15 min with 1 keV  $\text{Ar}^+$  ions at room temperature, yielding a target current of 50  $\mu\text{A}$  at a partial Ar pressure of approximately  $4 \times 10^{-5}$  mbar. After treatment, the surface was annealed for 10 min at 426 °C and then gradually cooled to room temperature. Subsequently, the chamber was backfilled with nitrogen. The substrates were stored under an Ar atmosphere and flame annealed under a butane/oxygen flame immediately before the adsorption experiments were carried out. The Au substrates fabricated from this procedure became hydrophobic, with a water contact angle of 114°. The static water contact angles of the sample surfaces were

measured at ambient temperature and humidity in air using an automated contact angle goniometer (CRUSS DSA 10-Mk2).

The Si(100) substrate was first cleaned by ultrasonication for 15 min in a 10 % solution of Decon90 in Milli-Q water. Each slide was rinsed 10 times with Milli-Q water and then dried under a nitrogen stream. The samples were ultrasonicated in dichloromethane for 15 min, removed, dried and then rinsed under Milli-Q water, after which they were immersed in piranha solution (70:30, v/v, H<sub>2</sub>SO<sub>4</sub>:H<sub>2</sub>O<sub>2</sub>) for 10 min<sup>18</sup>.

Consequently, a 2 nm thick oxide layer, whose surface was most likely terminated with the OH groups, formed on the Si substrates. The oxide surface became almost completely hydrophilic, with a water contact angle of less than 5°.

All of the chemicals were used without further purification. Calcium carbonate crystals were synthesized by gas diffusion following a previously reported method<sup>19</sup>. The synthesis was carried out in 50 mL glass bottles placed in a closed desiccator. The desiccator was placed in an oven at 60 °C for 24 h. In a typical preparation, 26 mM aqueous CaCl<sub>2</sub> solution was stirred for 15 min. The substrates were dipped vertically into the above-mentioned CaCl<sub>2</sub> solution. Each bottle was then covered with parafilm, punched with three needle holes and placed in a desiccator. Three small weighing bottles (10 mL) with crushed ammonium carbonate were also covered with parafilm punched with three needle holes and placed at the bottom of the desiccator. After different mineralization times, the parafilm was removed. The precipitate on the substrates were rinsed with deionized water and ethanol and allowed to dry at room temperature.

Crystals were collected and characterized by powder X-ray diffraction on a Bruker D8 advance diffractometer using Cu KR radiation ( $\lambda = 1.5406 \text{ \AA}$ ). The XRD patterns were observed between angles of 10° and 60°. Scanning electron microscopy images were taken using a KYKY-2000 instrument. Fourier transform infrared spectra were recorded at 4 cm<sup>-1</sup> resolution using a Bruker IFS-66 evacuated spectrometer.

## RESULTS AND DISCUSSION

Changes in the morphology of the produced CaCO<sub>3</sub> crystals were induced by the hydroxylated Si substrates (Fig. 1a). A few of the CaCO<sub>3</sub> particles are about 10  $\mu\text{m}$  in diameter and exhibit accumulated homogeneous rhombohedral crystals (Fig. 1a, 1b). Fig. 1c shows the SEM image of CaCO<sub>3</sub> grown on the Au substrate. The difference from that shown in Fig. 1a is the formation of cluster-like aragonite crystals.

The CaCO<sub>3</sub> phases in the Si and Au substrates were detected by XRD (Fig. 2). The XRD patterns of the CaCO<sub>3</sub> crystals grown on the Si substrate exhibit diffraction peaks at  $2\theta = 29.5^\circ$ ,  $36.1^\circ$ ,  $39.5^\circ$  and  $43.3^\circ$ , corresponding to calcite crystal faces (104), (110), (113) and (202), respectively. Moreover, a spot of vaterite forms on the Si substrate. The diffraction peaks occur at  $2\theta = 23.1^\circ$  and  $27.1^\circ$ , corresponding to vaterite crystal faces (100) and (101), respectively. The representative crystal face of vaterite is (101). However, when CaCO<sub>3</sub> crystallizes on the Au substrate, the maximum diffraction peak occurs at  $2\theta = 31.5^\circ$ , corresponding to aragonite crystal face (002). The other two peaks appear at  $37.9^\circ$  and  $45.9^\circ$ , corresponding to aragonite crystal faces (112) and (221). The strong peaks

appearing at  $31.5^\circ$  indicate that the interface between the crystallite and Au substrate may be the (001) face.

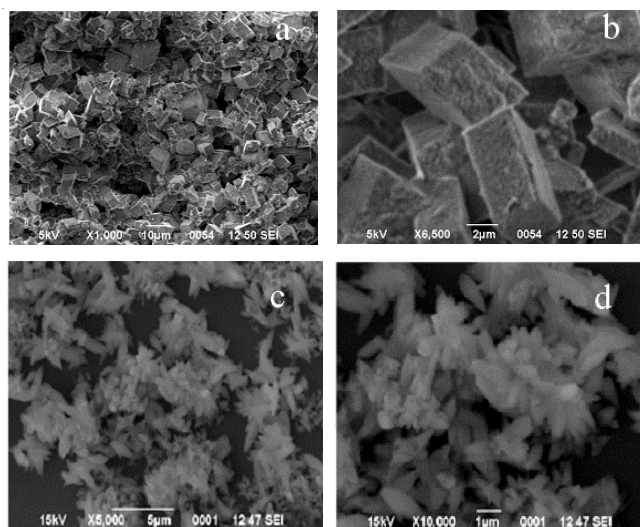


Fig. 1. SEM images of CaCO<sub>3</sub> crystals nucleated on the Si substrate (a), (b) and the Au substrate (c), (d)

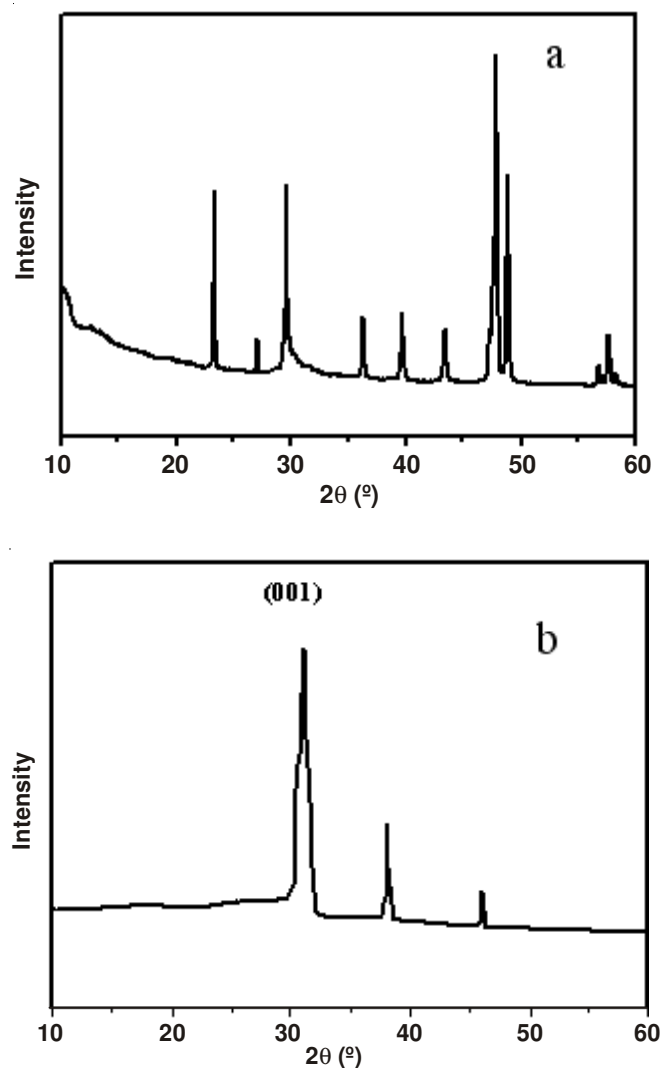


Fig. 2. XRD patterns of CaCO<sub>3</sub> crystals nucleated on the Si substrate (a) and the Au substrate (b)

The corresponding FTIR spectra are shown in Fig. 3. For the Si substrates, the XRD analysis indicates the presence of vaterite and calcite phases, as well as dominant crystalline precipitates. The FTIR spectra are also consistent with the results of XRD analysis, except for the pronounced peak at  $712\text{ cm}^{-1}$ , at which a broad absorption band is observed at  $745\text{ cm}^{-1}$ . This absorption band is the characteristic peak of crystalline vaterite<sup>20</sup>. For the Au substrate, absorption occurs at  $854\text{ cm}^{-1}$ ,  $713\text{ cm}^{-1}$ ,  $700\text{ cm}^{-1}$ , corresponding to the characteristic peaks of crystalline aragonite<sup>21</sup>.

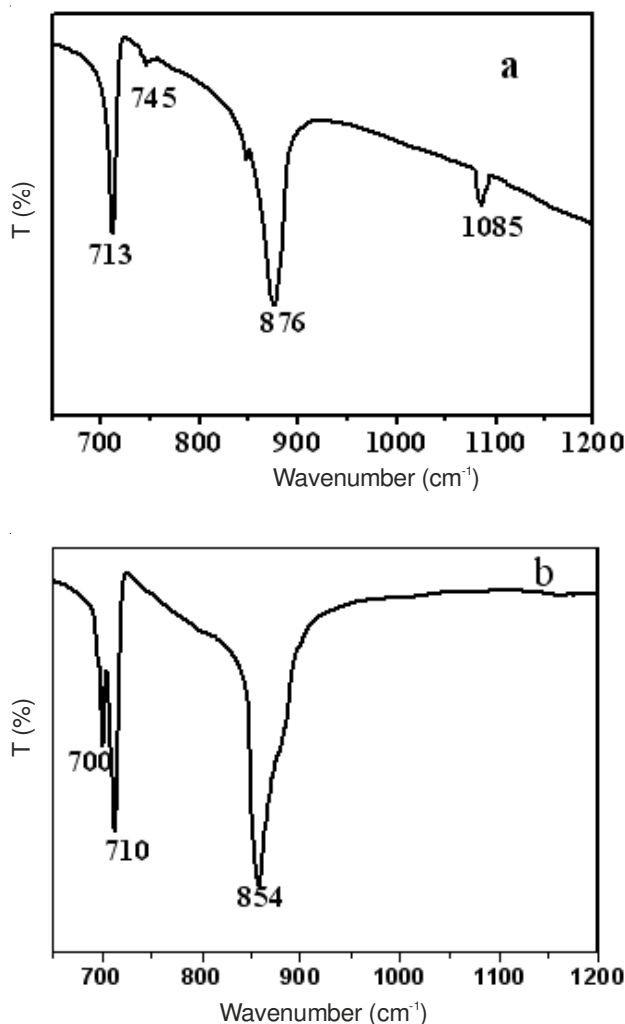


Fig. 3. FTIR spectra of  $\text{CaCO}_3$  crystals nucleated on the Si substrate (a) and the Au substrate (b)

In the present study, the crystallization process may be a heterogeneous nucleation process. When the solid template is positioned vertically in a solution, the absorption of solution-formed crystallites is difficult to realize because of gravity. In such cases, crystal growth on the solid film is controlled mainly by a heterogeneous nucleation process<sup>22</sup>.

Lattice matching<sup>23</sup>, degree of supersaturation<sup>24</sup> and electrostatic interactions<sup>25</sup> are important factors that induce the heterogeneous nucleation process. These can influence the process either individually or collectively as crystal growth is controlled.

The crystal formation mechanisms may also differ given the different physical and chemical properties of the solid

template. In this study,  $(\text{NH}_4)_2\text{CO}_3$  vapour diffusion proceeds at a slow rate and the overall supersaturation is relatively low. The precipitate is composed exclusively of calcite in the absence of a substrate. The above-mentioned results clearly show that the vaterite and calcite polymorphs co-crystallize on the hydroxylated Si template. Being inherently unstable and highly soluble, vaterite may not be abundant in nature. However, this phase has been reported to exist for long periods in some biological systems. The kinetic stabilization of vaterite is achieved primarily through the involvement of acidic macromolecules such as proteins and polysaccharides. Several potential factors can be suggested for vaterite formation in the hydroxylated Si template.

First, the substrate used (*i.e.*, the hydroxylated Si substrate) has a natural silicon oxide surface presenting silanol (OH) groups and shows negatively charged properties. As a negative substrate, the Si substrate can capture  $\text{Ca}^{2+}$  through OH, thereby causing the local enrichment of calcium ions. Upon the introduction of  $\text{CO}_3^{2-}$  and diffusion into the solution, vaterite crystalline distributions are enriched by  $\text{Ca}^{2+}$  ions around the Si substrate. According to Ostwald's rule<sup>26</sup>, the metastable crystalline form tends to precipitate under high local supersaturation, resulting in the formation of vaterite crystals around the substrate. Furthermore, the vaterite crystals adsorb onto the Si substrate upon electrostatic interaction, thereby retarding the transformation of the crystal into more stable crystalline forms.

The density of the hydroxyl group may be another factor that plays an important role in forming and stabilizing the vaterite phase. Previous reports showed that the high density of carboxylic groups on carboxyl-functionalized multiwalled carbon nanotubes<sup>27</sup> can strongly interact with  $\text{Ca}^{2+}$  and prevent vaterite dissolution, thereby stabilizing the vaterite phase. However in case of mica<sup>16</sup>, however, no hydroxyl groups can interact with  $\text{Ca}^{2+}$  to form nucleation sites and stabilize the vaterite phase and vaterite can easily dissolve in water and transform into calcite crystals. Because of faint acidity, the silanol group does not act as a carboxylic group and may partly stabilize the vaterite phase. Therefore, the  $\text{CaCO}_3$  formed on the hydroxylated Si is the result of calcite and vaterite co-formation.

As for  $\text{CaCO}_3$  crystallized on the Au template, the formation of aragonite can be explained using the potential lattice matching relationship at the template/crystal interface. As discussed above, the face of aragonite at the template/crystal interface is the (001) face. According to the small-angle diffraction (Fig. 4) obtained in this study, the (110) projection of Au atoms exhibits rectangular lattice constants of 4.01 and 2.8 Å. The result shows that the Au(110) surface is predominately in the  $(1 \times 1)$  structure, which is characterized by rows of Au atoms separated by 2.8 Å along the row and separated from adjacent parallel rows by 4.01 Å. This structure is lower than that of previous report<sup>28</sup>. Aragonite  $\text{CaCO}_3$  is known to crystallize in an orthorhombic crystalline<sup>29</sup> lattice with lattice constants of  $a = 4.9623\text{ Å}$ ,  $b = 7.968\text{ Å}$  and  $c = 5.7439$ . In comparison, the superimposition of a rectangular lattice ( $a_1$ ) 8.42 Å and ( $a_2$ ) 2.88 Å of the Au(110) substrate on the (001) face (4.9623 Å, 7.968 Å) of aragonite  $\text{CaCO}_3$  crystal induces good lattice matching. The mismatch along the a and b directions in the Au substrate are 3 and 14 %, respectively.

Oriented overgrowth can be achieved with a lattice mismatch approaching 30 %<sup>30</sup>. Aragonite crystals are obtained when the Au(110) substrate is dipped into the solution.

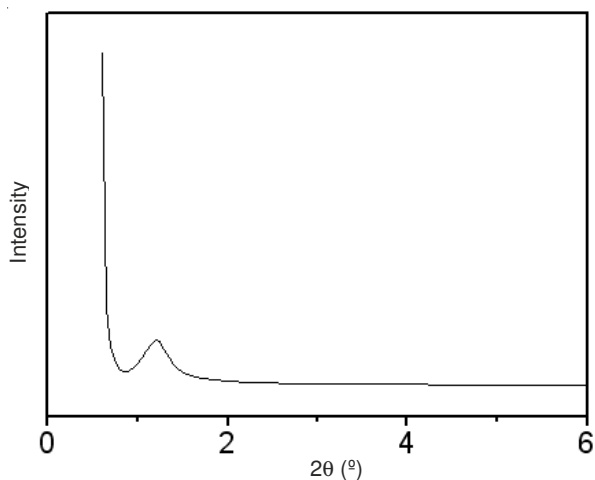


Fig. 4. Small-angle diffraction pattern of the Au substrate

Krampitz and Graser<sup>31</sup> and Meenakshi *et al.*<sup>32</sup> revealed that aragonite forms in nacre shells because of existing hydrophobic protein molecules. Recently, Rautaray *et al.*<sup>33</sup> used hydrophobic aerosol OT thin films as templates for the room temperature synthesis of aragonite crystals. Lee *et al.*<sup>34</sup> synthesized aragonite crystals in a hydrophobic anodic aluminum oxide membrane template. Therefore, the hydrophobic nature of the Au template may be a possible reason for aragonite formation.

### Conclusion

As crystallization parameters for the biomineralization of CaCO<sub>3</sub>, the solid substrates impose considerable effects on the crystal growth process. When CaCO<sub>3</sub> crystal growth is induced by the Si substrate, vaterite and calcite polymorphs co-form, whereas the Au substrate induces aragonite crystal growth. The crystal growth mechanism differs with varied substrates. As a negative template, the Si substrate features the electrostatic interaction and density of the hydroxyl group as the primary factors responsible for controlling the crystallization of CaCO<sub>3</sub> on the template. For the Au substrate, the lattice matching factor and hydrophobicity play an important role in the growth of aragonite crystal.

### ACKNOWLEDGEMENTS

The authors are grateful for the financial support provided by the Natural Science Foundation of China (No. 30570235, 50635030), Fok Ying Tong Education Foundation (No. 101020) and the Jilin Science and Technology Development Project (No. 20111808).

### REFERENCES

1. M. Brian, J.Z. Michael and J. Zaworotko, *Chem. Rev.*, **101**, 1629 (2001).
2. H.G. Brittain, *J. Pharm. Sci.*, **99**, 3648 (2010).
3. E. Weber, in ed.: M.R. Caira, Design of Organic Solids, Springer: Berlin, New York, NY, Chapter 6, pp. 163-208 (1998).
4. X.Q. An, C.B. An and C. Chuanbao, *J. Phys. Chem. C*, **112**, 6526 (2008).
5. F. Manoli and E. Dalas, *J. Cryst. Growth*, **217**, 416 (2000).
6. E. Zolotoyabko and B. Pokroy, *Cryst. Eng. Commun.*, **9**, 1156 (2007).
7. Y. Zhao, Y. Lu, Y. Hu, J.P. Li, L.A. Dong, L.N. Lin and S.H. Yu, *Small*, **6**, 2436 (2010).
8. Y.Y. Kim, E.P. Douglas and L.B. Gower, *Langmuir*, **23**, 4862 (2007).
9. J.R.I. Lee, T.Y.J. Han, T.M. Willey, D. Wang, R.W. Meulenberg, R.J. Nilsson, P.M. Dove, L.J. Terminello, T. van Buuren and J.J. De Yoreo, *J. Am. Chem. Soc.*, **129**, 10370 (2007).
10. P. Pichon Benoît, H.H. Bomans Paul, M. Frederik Peter, A.J.M. Sommerdijk and Nico, *J. Am. Chem. Soc.*, **130**, 4034 (2008).
11. Erman, D.J. Ahn, A. Lio, M. Salmeron, A. Reichert and D. Charych, *Science*, **269**, 515 (1995).
12. D.D. Archibald, S.B. Quadri and B.P. Gaber, *Langmuir*, **12**, 538 (1996).
13. M. Addadi, J. Moradian, E. Shay, N.G. Maroudas and S. Weiner, *Proc. Natl. Acad. Sci. USA*, **84**, 2732 (1987).
14. J.J.J.M. Donners, R.J.M. Nolte and N.A.J.M. Sommerdijk, *J. Am. Chem. Soc.*, **124**, 9700 (2002).
15. Y.J. Han and J. Aizenberg, *Angew. Chem. Int. Ed.*, **42**, 3668 (2003).
16. C.J. Stephens, Y. Mouhamad, F.C. Meldrum and H.K. Christenson, *Cryst. Growth Des.*, **10**, 734 (2010).
17. M. Weinhold, S. Soubatch, R. Temirov, M. Rohlffing, B. Jastorff, F.S. Tautz and C. Doose, *J. Phys. Chem. B*, **110**, 23756 (2006).
18. K.M. Shley, J.C. Meredith, E. Amis, D. Raghavan and A. Karim, *A. Polymer*, **44**, 769 (2003).
19. S.S. Wu, H.Q. Cao, S.F. Yin X.R. and V. Chernow, *Inorg. Chem.*, **48**, 10326 (2009).
20. R.B. Frankel and S. Mann, S. Encyclopedia of Inorganic Chemistry; John Wiley & Sons Ltd.: Chichester, Vol. **1**, (1994).
21. N. Nassrallah-Aboukais, A. Boughriet, J. Laureyns, A. Aboukais, J.C. Fischer, H.R. Langelin and M. Wartel, *Chem. Mater.*, **10**, 238 (1998).
22. F. Lu, X. Zhao, G. Zhou a, H.S. Wang and Y. Ozaki, *Chem. Phys. Lett.*, **458**, 67 (2008).
23. H.G. Haubruge, R. Daussin, A.M. Jonas, R. Legras, J.C. Wittmann and B. Lotz, *Macromolecules*, **36**, 4452 (2003).
24. T.V. Bykov and X.C. Zeng, *J. Chem. Phys.*, **125**, 144515 (2006).
25. K. Allain, R. Bebaee and S. Lee, *Cryst. Growth Des.*, **9**, 3183 (2009).
26. P.R.T. Wolde and D. Frenkel, *Phys. Chem. Chem. Phys.*, **1**, 2191 (1999).
27. W. Li and C. Gao, *Langmuir*, **23**, 4575 (2007).
28. C.P. Mansley, C.I. Smith, A. Bowfield, D.G. Fernig, C. Edwards and P. Weightman, *J. Chem. Phys.*, **132**, 214708 (2010).
29. B. Pokroy and E. Zolotoyabko, *Chem. Commun.*, p. 2140 (2005).
30. J.H. Fendler and F.C. Meldrum, *Adv. Mater.*, **7**, 607 (1995).
31. G. Krampitz and G. Graser, *Angew. Chem. Int. Ed. Engl.*, **27**, 1145 (1988).
32. V.R. Meenakshi, P.E. Hare and K.M. Wilbur, *Comp. Biochem. Physiol.*, **40**, 1037 (1971).
33. D. Rautaray, S.R. Sainkar and M. Sastry, *Chem. Mater.*, **15**, 2809 (2003).
34. I. Lee, H. Han and S.-Y. Lee, *J. Cryst. Growth*, **312**, 1741 (2010).